NASA TN D-1814

22p

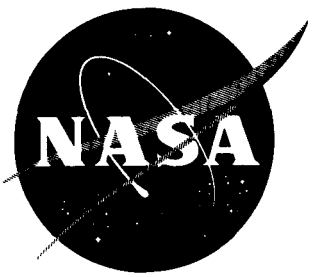

TECHNICAL NOTE

D-1814

AN EXPERIMENTAL EVALUATION OF THREE TYPES OF THERMAL PROTECTION MATERIALS AT MODERATE HEATING RATES AND HIGH TOTAL HEAT LOADS

By Andrew J. Chapman

Langley Research Center
Langley Station, Hampton, Va.

NATIONAL AERONAUTICS AND SPACE ADMINISTRATION
WASHINGTON
July 1963

NATIONAL AERONAUTICS AND SPACE ADMINISTRATION

TECHNICAL NOTE D-1814

AN EXPERIMENTAL EVALUATION OF THREE TYPES OF THERMAL PROTECTION MATERIALS AT MODERATE HEATING RATES AND HIGH TOTAL HEAT LOADS

By Andrew J. Chapman

SUMMARY

Three types of materials have been tested in an electric-arc-heated airstream to compare their performance as thermal protection systems for reentry applications involving long heating periods and high total-heat loads. Test stream conditions and the specimen configuration were held constant for all tests. The quantity of heat dissipated by a specimen while its back-surface temperature was limited to a given value was used as a criterion for evaluating the materials. The tests indicated that charring composite materials were more effective than porous ceramic materials with an ablative filling or than low-temperature ablating materials.

INTRODUCTION

A manned vehicle returning to earth at supercircular velocity will require an extended period to reenter the atmosphere in order to keep deceleration forces caused by aerodynamic drag below the limit of human tolerance. The resulting aerodynamic heating will require the use of a thermal protection system which can efficiently reduce the transfer of heat to the vehicle over a long period of time.

A method which is currently of interest for reducing aerodynamic heating is the use of a surface material which will dissipate heat either by ablating, radiating at a high temperature, or by both processes simultaneously. Heat which is not dissipated by such processes is accumulated within the shield material and conducted toward the main vehicle structure. Conduction of accumulated heat increases with the length of the heating period and becomes a major problem in the periods associated with manned reentry.

Examples of materials in the first category mentioned above are polymers such as nylon and Teflon which melt or sublime at comparatively low temperatures; examples of the second category are ceramic materials which can maintain the higher surface temperatures at which radiation is effective. The third category is represented by compositions of organic materials which decompose at relatively low temperatures while producing a high-temperature char-surface residue, and

compositions consisting of a ceramic matrix filled with an organic material. Investigations of such materials have been reported in references 1 to 6. In the present investigation a comparative evaluation was made to determine the relative thermal shielding performance of low-temperature, ceramic, and charring composite materials and to indicate the most effective combination of component materials for each of these classes. The test flow environment was produced by an electric-arc-heated air jet. Because of the complexity of the thermal shielding process, a simplified criterion was used to evaluate the shielding performance. This criterion was the quantity of heat dissipated by a unit weight of material while the back-surface temperature was limited to a given value, with model configuration and test-stream conditions maintained approximately constant for all tests.

SYMBOLS

c_p	specific heat at constant pressure
m	material specimen unit weight, lb/sq ft
Q_o	total cold-wall heat load, Btu/sq ft
Q_o/m	effective heat capacity, Btu/lb
Q_B	total heat transferred to back surface of material specimen, Btu/sq ft
$\bar{q}$	average cold-wall heat-transfer rate for exposure period in test stream, Btu/sq ft-sec
T	temperature, ^oF
ΔT	back-surface sensor temperature rise, ^oF
$(dT/dt)_f$	maximum rate of temperature rise at termination of exposure, ^oF/sec
t	time, sec
ρ	density, lb/cu ft
τ	thickness of metal calorimeter, ft

Subscripts:

a	quantity ablated
cu	properties of copper

f	value at end of exposure in test stream
max	maximum value or time at which maximum occurs

TEST FACILITY

The performance of the thermal protection materials was evaluated in the 2500-kilowatt arc jet at the Langley Research Center. This facility with the inserter mechanism which positioned the material specimen is shown in figure 1.

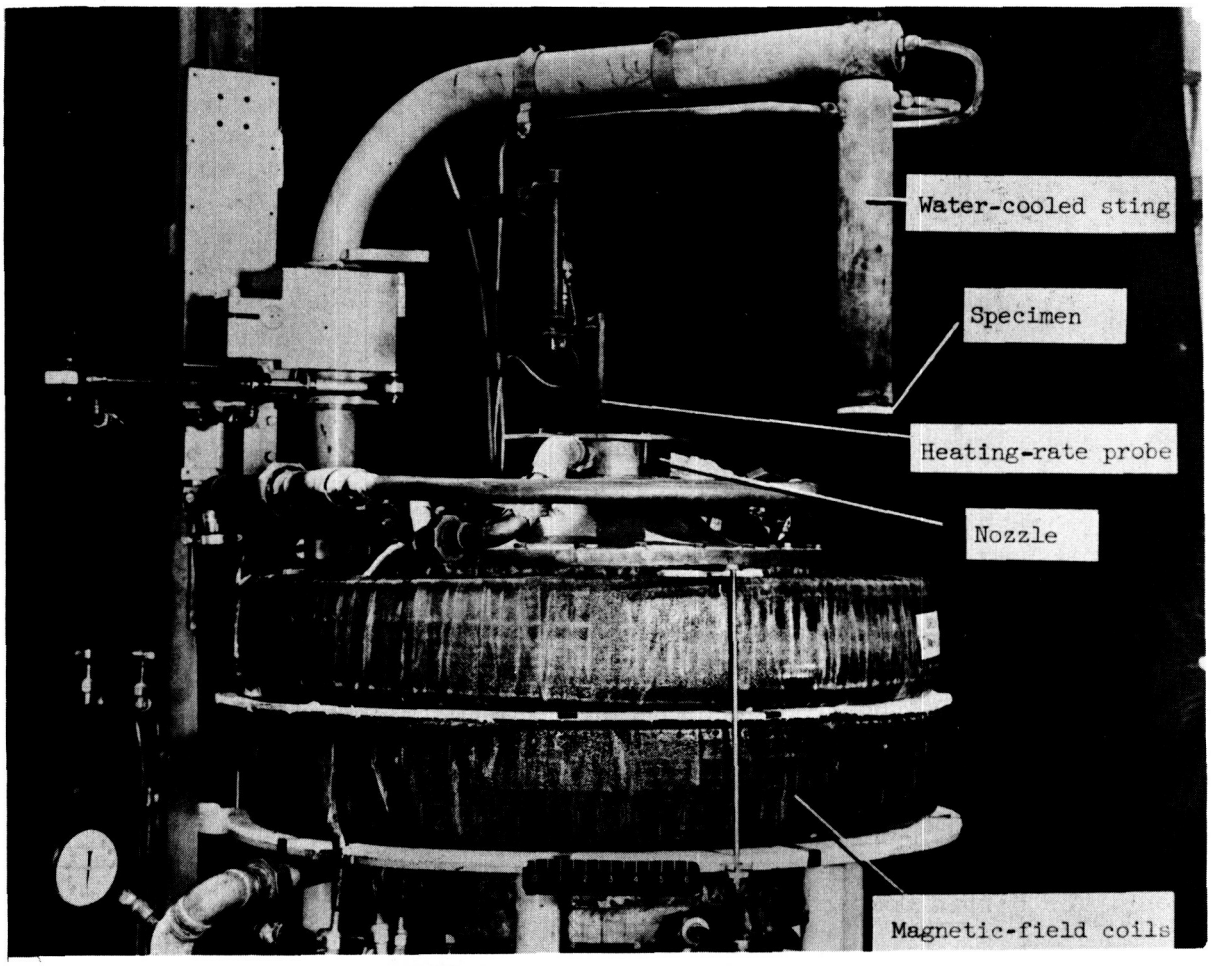

Figure 1.- The 2500-kilowatt arc jet at the Langley Research Center. L-61-3423.1

The concentric-ring electrodes, which are shown in figure 2, were constructed of copper tubing and were cooled by water circulating through the tubing under pressure. Each electrode set was energized by one phase of a three-phase alternating-current power source, and the arc formed between the concentric rings was rotated in the plane of the rings by a magnetic field produced by the coils surrounding the arc chamber. Air was directed into the arc chamber at the base of each electrode set and was heated by the arc as it passed through the electrode rings.

The heated airstream which passed through the 4-inch-diameter nozzle at the top of the arc chamber was uncontaminated except for a small amount of copper (approximately 0.025 percent by weight of airflow). Characteristics of the test stream for the present investigation are given in table I.

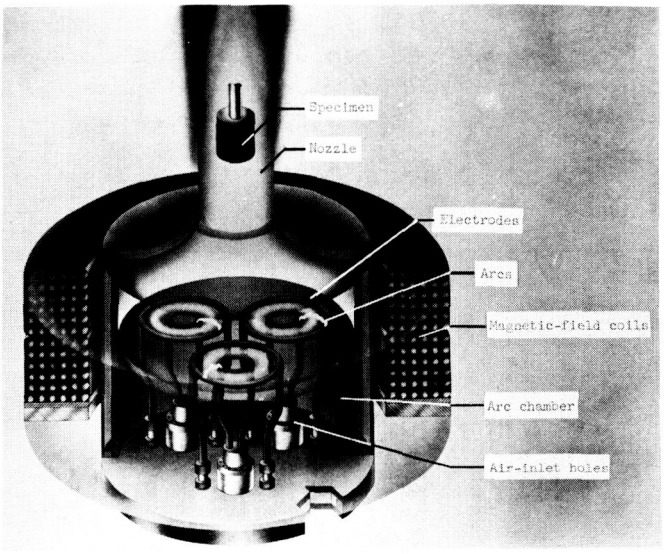

L-62-99

Figure 2.- Phantom view of 2500-kilowatt arc jet.

The test environment approximately simulated the conditions behind a normal shock wave on a vehicle traveling with a velocity of 12,000 ft/sec at an altitude of 120,000 feet. These conditions correspond to the terminal portion of reentry initiated at parabolic velocity. The test enthalpy of 3,000 Btu/lb was approximately one-eighth of that associated with maximum heating conditions, and the test heating rate of 100 Btu/ft^2-sec was approximately one-fifth of the peak convective heating rate for this type reentry. However, previous investigations have shown that ablation performance will improve with increasing enthalpy (refs. 1, 2, and 3) and will also improve with increasing heating rate for materials which have a surface capable of maintaining high temperatures at which radiation is effective (ref. 6).

MATERIALS AND SPECIMENS

The thermal shielding materials which were investigated may be considered to belong to one of three general classes: charring composite materials, ceramic materials, and low-temperature materials. Some of these materials were fabricated by the Langley Research Center and some were obtained commercially. In addition, a large number of specimens were supplied by the following companies: Avco Research and Advanced Development Division, Chance Vought Corp., The Emerson Electric Manufacturing Company, General Electric Missile and Space Vehicle Department, The Martin Company, and Narmco Industries, Incorporated.

Charring Composite Materials

The charring composites had as a primary component an organic material such as phenolic or epoxy resin which decomposed at a comparatively low temperature and produced the characteristic carbonaceous surface residue. Many of the charring composites also contained organic and inorganic additives to improve their thermal and physical characteristics.

The charring composite materials which were investigated are listed in table II. Component materials are listed in the second column whenever these are known. The percent composition by weight is given for the materials fabricated by the NASA Langley Research Center. For some materials, data are shown for two tests.

Ceramic Materials

The ceramic materials consisted of a foamed or porous ceramic base such as zirconia, alumina, silicon carbide, or silica. Several of the silicon carbide base materials had a coating of zirconia. Most of the porous ceramics were filled with an organic material such as epoxy or phenolic resin; however, several ceramic materials without an organic filling were tested.

The ceramic materials are listed in table III in the same manner used in table II. The first component listed in the second column for each material is the basic ceramic matrix.

Low-Temperature Materials

The low-temperature materials consisted of the polymers Teflon, nylon, polyethylene (all of which were obtained commercially), and Avcoat 5019 (a proprietary product of the Avco Research and Advanced Development Division). These materials are listed in table IV in the same manner used in tables II and III.

Specimen Configuration and Instrumentation

The material specimens were flat disks which had a diameter of 3 inches, a thickness determined by the density of the material, and a unit weight of 3 lb/sq ft. This unit weight was used in order to obtain an exposure period in which steady-state ablation and conduction conditions would be approached in most tests, and, at the same time, to avoid a large specimen thickness which would cause a noticeable effect of two-dimensional heat transfer. The thickness of the specimens varied from 0.26 inch for Teflon to 1.00 inch for the lower density phenolic nylon compositions.

The specimen assembly consisted of the material specimen with a brass mounting ring and a copper sensor bonded to the back surface as shown in figure 3. The bonding material was General Electric RTV-90, a room-temperature vulcanizing silicone rubber. The back-surface sensor consisted of a 0.125-inch-thick copper disk and a concentric ring with thermocouples attached in the positions shown in figure 3.

Heat transfer through the specimen was indicated by the temperature and heat capacity of the center disk which acted as a calorimeter. The temperature rise indicated by the thermocouple on the center disk or calorimeter will subsequently be referred to as the back-surface temperature rise. The concentric guard ring provided even distribution of the heat-sink effect on the back surface of the

specimen and was physically separated from the calorimeter to limit radial conduction of heat through the sensor. Reduction of heat transfer from the front surface of the material specimen to the back-surface sensor simulated the effect of an actual heat shield on a vehicle structure. The water-cooled sting (fig. 3), on which the specimen assembly was mounted, prevented transfer of heat from the test stream to the back surface of the specimen.

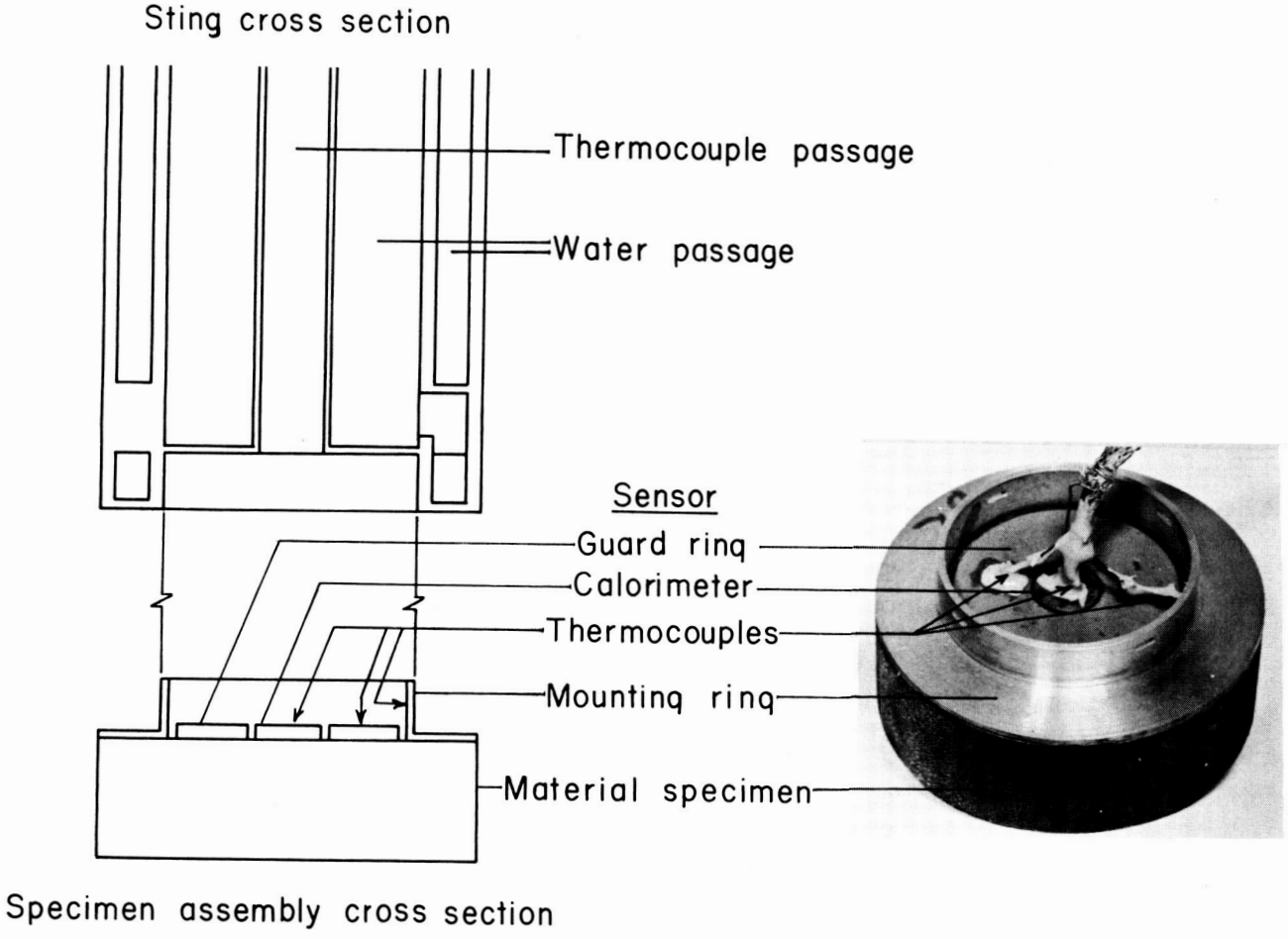

Figure 3.- Material specimen instrumentation and mounting detail. L-61-1778

TEST PROCEDURE

To begin a test the arc jet was operated for a short time to permit stream conditions to stabilize, after which the heating-rate probe was inserted into the test stream. The heating rate was measured for a few seconds and recorded oscillographically. When it was determined that the proper heating rate was being obtained, the inserter was actuated to move the probe out of the test stream and to position the sting and specimen assembly in the stream. Temperatures on the back-surface sensor were recorded oscillographically throughout exposure and the

specimen was removed from the test stream when the temperature of the center disk, or calorimeter, reached 300° F above room temperature. After the specimen was removed, the heating-rate probe was reinserted into the stream for a few seconds and then the jet was stopped. All sensor temperatures were recorded after exposure had terminated until a maximum temperature on the calorimeter was indicated and a definite decrease noted.

Heating-Rate Measurement

Heating rate in the test stream was measured by a 3/8-inch-diameter probe which was constructed according to the design presented in reference 7. The heating-rate probe is shown in position over the nozzle of the arc jet in figure 1 and is shown in detail in figure 4. A copper nickel alloy disk forms the face of the probe which is placed normal to the direction of the stream. The disk is silver-soldered around its periphery to the copper plug at the end of the water cooling jacket. A thermal flux on the disk generates a heat flow radially from the center of the disk to the cooler copper plug. The copper wire attached to the center of the back surface of the disk is a thermocouple hot junction, and the connection between the disk and the copper plug is the cold junction. The output indicated by the thermocouple is calibrated by using a source of known heating rate, and this calibration is applied to the output of the probe when it is exposed in the test stream.

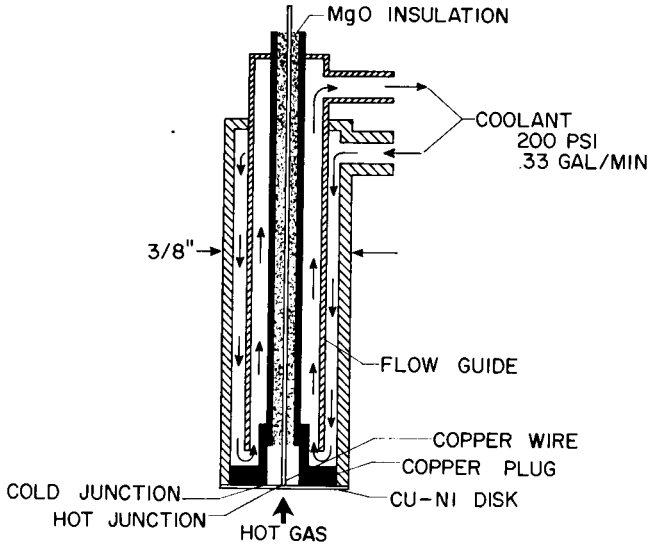

Figure 4.- Probe for measuring heat-transfer rate in arc-heated airstream.

The heating rate measured on the 3/8-inch-diameter probe was correlated with that measured on a probe of shape and size (3-inch diameter) identical to the material specimens. The front surface of the full-scale probe was a thin stainless-steel plate with thermocouples attached to the unexposed side. Heating rate was determined from the heat capacity of the stainless-steel plate and the initial rate of temperature rise which occurred when the probe was momentarily exposed in the test stream.

Calibration of Test Stream

Static temperature of the test stream was measured by a spectrographic technique based on the ratio of intensities of two lines of the copper spectrum. This method is described in reference 8. It was possible to use this method because of the trace of copper in the stream which was described in the section entitled "Test Facility." The free-stream enthalpy was determined from the static

temperature at a pressure of 1 atmosphere by using a Mollier chart for air in chemical equilibrium. The stagnation enthalpy was approximately equal to the free-stream enthalpy because the energy derived from the velocity of the stream was a very small part of the total stream energy.

RESULTS AND DISCUSSION

Test results of primary interest were obtained in the form of back-surface-temperature histories. Typical temperature histories which represent the range of performance of each class of material are shown in figures 5 to 7. The back-surface temperature data for each test are presented in tables II, III, and IV. These are the times at which the back-surface sensor indicated temperature rises of 50° F and 300° F, the total exposure time, the back-surface-temperature rise at termination of exposure, the rate of temperature rise at the termination of exposure, and the maximum temperature rise with the time at which this maximum occurred. Curves similar to the typical curves shown in figures 5, 6, and 7 could be sketched from this tabular information.

The maximum temperature rise occurred after termination of exposure and was an indication of the total quantity of heat transferred through the material specimen. The total back-surface heat load may be calculated from the maximum temperature rise and the heat capacity of the calorimeter as shown in the section entitled "Data Evaluation." Temperature-history data following the termination of exposure are not given for tests where the material was completely ablated, because the sensor temperature did not indicate heat transferred through the material specimen when the sensor was exposed directly to the test stream.

Tables II, III, and IV also present the percent weight loss during exposure for each material specimen, the average cold-wall heating rate, total cold-wall heat load, and the effective heat capacity which was the primary criterion for

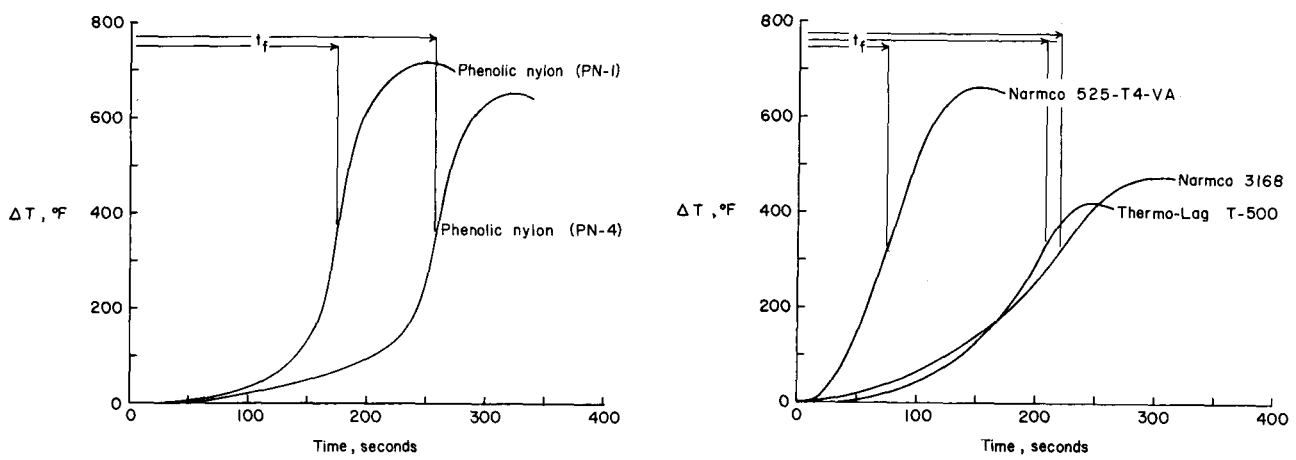

(a) Low-density materials ($\rho < 80$ lb/cu ft). (b) High-density materials ($\rho > 80$ lb/cu ft).

Figure 5.- Typical back-surface-temperature histories for charring composite materials.

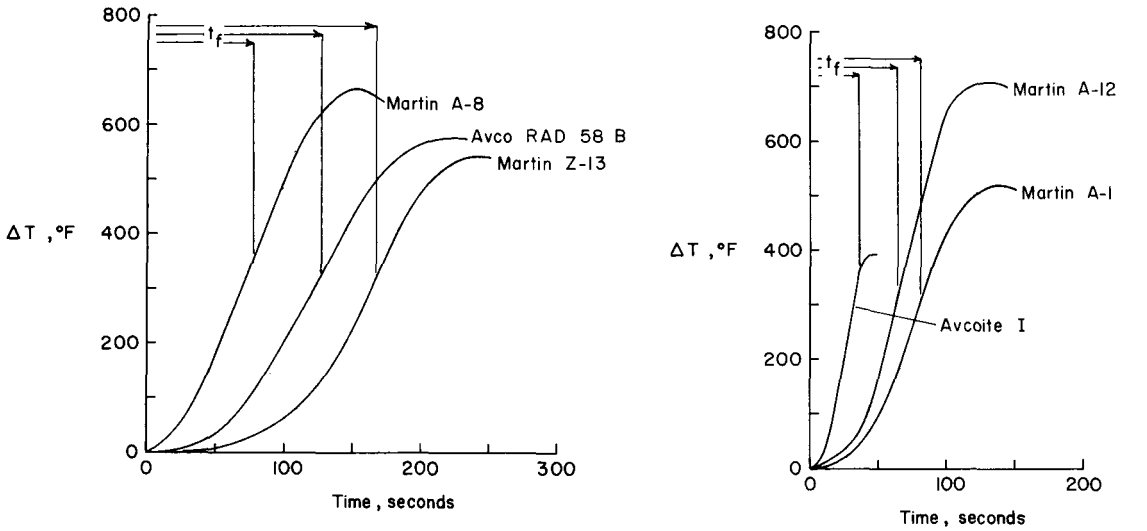

(a) Ceramic materials with ablative filling.

(b) Unfilled ceramic materials.

Figure 6.- Typical back-surface-temperature histories for ceramic materials.

evaluating thermal-shielding performance. The tests are arranged in order of decreasing values of the effective heat capacity.

Data Evaluation

In order to make a direct comparison of material performance, the following procedure was used. Test stream conditions, heating rate, specimen configuration, and specimen unit weight were maintained approximately constant in all tests, and exposure in the test stream was terminated at a back-surface-temperature rise of approximately 300° F. On this basis, performance was evaluated according to the quantity of heat dissipated by a unit weight of material:

$$\text{Effective heat capacity} = \frac{Q_o}{m} \qquad (1)$$

The choice of a 300° F back-surface-temperature rise was arbitrary; however, it represented maximum performance for many materials which had only a thin layer of residual char remaining over the sensor when this temperature rise was indicated.

The total cold-wall heat load was obtained from the exposure time and the average heat-transfer rate for the exposure period

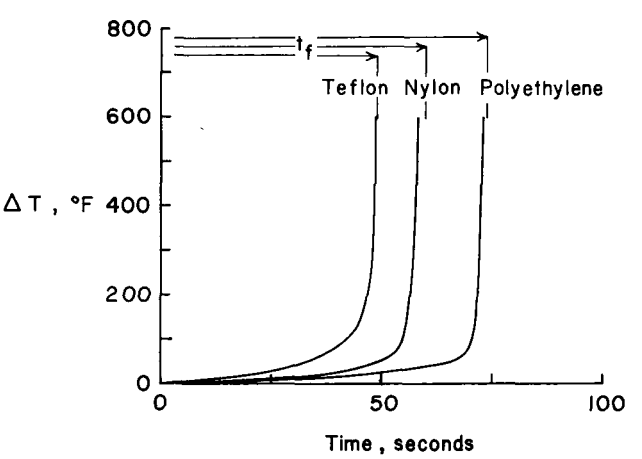

Figure 7.- Typical back-surface-temperature histories for low-temperature ablation materials.

$$Q_o = t_f \bar{q} \tag{2}$$

Normally there was only a small variation between the values of heating rate measured before and after specimen exposure.

The heating rate at the back surface of the material specimen or the total heat transferred to the back surface at any time may be obtained from the product of the sensor heat capacity and the rate of temperature rise or the total temperature rise, respectively. For example, the total heat transferred to the back surface of the material specimen is:

$$Q_B = \left(c_p \rho \tau\right)_{cu} \Delta Tm \tag{3}$$

where the heat capacity of the 0.125-inch-thick copper calorimeter was

$\left(c_p \rho \tau\right)_{cu} = 0.544$ Btu/sq ft-$^\circ$R.

As previously indicated, exposure was terminated at a back-surface-temperature rise of approximately 300° F. However, in many cases the temperature rise at the termination of exposure was actually greater than 300° F as a result of the high rate of temperature rise near termination and also as a result of a delay of a few seconds in removing the specimen from the stream. The difference between the time for a 300° F temperature rise and termination of exposure was in most cases not more than 5 seconds. In all cases Q_o and Q_o/m were calculated by using t_f instead of t for $\Delta T_f = 300^\circ$ F. The differences in t_f and t for $\Delta T = 300^\circ$ F resulted in variations in Q_o/m of less than 3 percent for the more effective materials to more than 10 percent for the less effective materials. Values of t for $\Delta T = 300^\circ$ F are tabulated in tables II, III, and IV and values of Q_o/m for a common ΔT of 300° F may be determined if desired.

Behavior of Materials

Several characteristics of the shielding process are shown by the information in tables II, III, and IV, and by the typical temperature-history curves in figures 5, 6, and 7. High overall shielding effectiveness is indicated by a high value of Q_o/m. In addition, good insulating properties are indicated by a low initial rate of temperature rise (a long period for a 50° F temperature rise). For materials with good insulating properties a steep temperature gradient existed within a thin layer behind the char-uncharred material interface as a result of slow temperature penetration. Consequently most of the materials with good insulating properties experienced a high total-mass loss before the back-surface-temperature rise approached 300° F, and this resulted in a relatively high final rate of temperature rise $(dT/dt)_f$.

A comparatively high initial rate of temperature rise indicated less effective insulating properties. For materials exhibiting this kind of temperature history, the rate of temperature penetration into the uncharred material was relatively high and resulted in a back-surface-temperature rise of 300° F before

a high total-mass loss had occurred. The rate of temperature rise at termination of exposure was usually moderate compared with that for good insulating materials and increased gradually over the exposure period rather than accelerating abruptly near termination.

Charring composite materials.- A comparison of the range of values of Q_o/m in tables II, III, and IV, shows that charring composite materials were more effective as a class than the ceramic or the low-temperature materials. The most effective charring composite materials were based on phenolic resin, part of which was in the form of phenolic Microballoons. These materials also contained a large percentage of nylon which improved performance by increasing transpiration (ref. 3) and absorption shielding (ref. 5). The inclusion of a small amount of silica, in the form of Eccospheres or fiber, improved char integrity. Composites based on epoxy resin with similar additives were also effective.

Back-surface-temperature histories are shown in figure 5 for several charring composite materials which represent maximum and minimum boundaries of performance, as well as typical intermediate values. Temperature histories for materials of relatively low density are shown in figure 5(a), while temperature histories for higher density materials are shown in figure 5(b). Reducing the density of the materials improved insulation characteristics and was important in achieving high performance in many cases. The four most effective charring composites had density values between 35 and 40 lb/cu ft and demonstrated good insulating characteristics by a low-temperature rise over most of the period of exposure (table II). These materials experienced comparatively high total-mass loss (m_a/m = 79 to 97 percent), which resulted in sharply accelerating temperature-rise rates near termination of exposure.

The least effective charring composites had high-density values, poor insulating characteristics, and low total-mass loss. However, several high-density materials demonstrated comparatively good performance. For example, Narmco 3168 and Thermo-Lag T-500 which had density values of 83 and 86 lb/sq ft, respectively, had effective heat capacities Q_o/m of 8,370 and 7,490 Btu/lb. Though low density is important for achieving high thermal-shielding performance, it appears that comparatively good performance can be obtained with higher density materials.

The exposure periods which terminated at a 300° F back-surface-temperature rise resulted in most of the charring composite materials being completely reduced to char. Photographs of several representative charring materials in figure 8 show the residual char in comparison to the original specimen. Though only a thin layer of char remained for phenolic-nylon (PN-4) and Thermo-Lag T-500, the sensor was completely covered by char at the end of exposure. The comparatively thick layer of residual material for Narmco 3168 was also composed entirely of char. Recent test results have indicated that the present test environment produces greater char-layer oxidation than an actual reentry flight condition (ref. 5).

Ceramic materials.- As a class, ceramic materials were less effective than charring composite materials. This may be seen by comparing maximum values of effective heat capacity Q_o/m in tables II and III. However, it is also shown that several filled ceramic materials were more effective than many

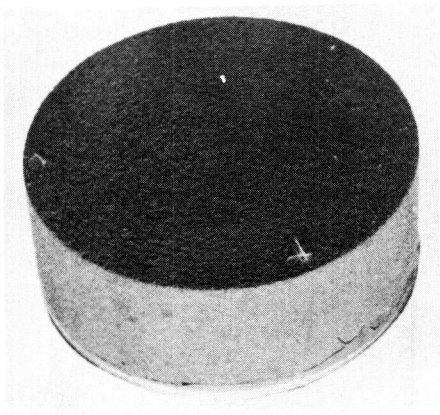

Phenolic nylon (PN-4)

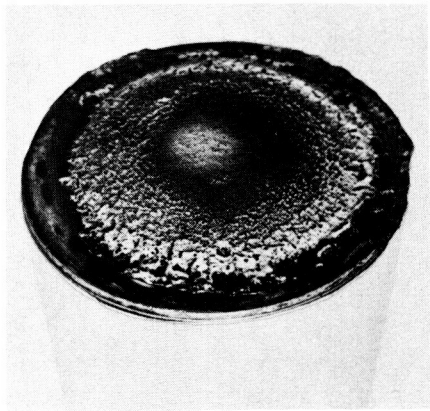

Before test

After test

Thermo-Lag T-500

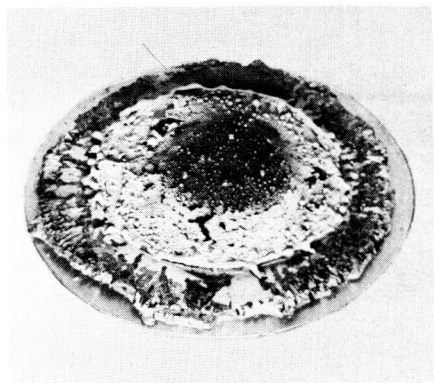

Before test

After test

Narmco 3168

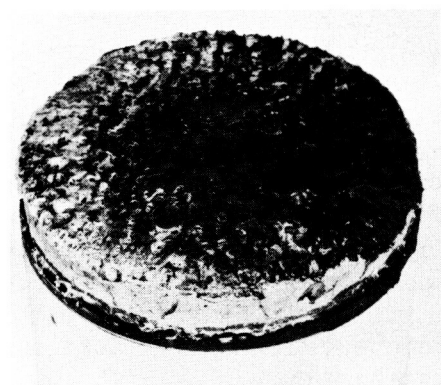

Before test

After test

Figure 8.- Typical charring composite materials. L-63-99

low-performance charring materials. Typical back-surface-temperature histories are shown in figure 6(a) for ceramic materials with an ablative filling and in figure 6(b) for unfilled ceramic materials.

The most effective ceramic materials evaluated in this investigation consisted of foamed zirconia filled with epoxy resin. Foamed zirconia and foamed silicon carbide filled with phenyl-silane or phenolic resin also were effective. Several unfilled foamed ceramic materials such as low-density silicon carbide and alumina were more effective than several filled ceramic materials. The most effective filled ceramic materials had comparatively high density (from 70 to 97 lb/cu ft) and a high content by weight of ablative materials, while the most effective unfilled ceramics were of low density (17 to 36 lb/cu ft). All the ceramic materials demonstrated comparatively high thermal-conductivity characteristics, which may be seen in table III by the comparatively short time for a 50° F temperature rise and which is illustrated by the typical temperature-history graphs in figure 6.

Photographs of several typical ceramic materials before and after exposure are shown in figure 9. The residual material was usually an integral layer of ceramic, as shown, even though several filled ceramic materials experienced a total mass loss of 75 percent or greater.

Low-temperature materials.- In table IV it is shown that all low-temperature materials experienced practically complete ablation before termination of exposure. This resulted in the sensors being exposed to the test stream so that meaningful data following termination of exposure could not be obtained. From the range of Q_o/m shown in table IV, it may be seen that the low-temperature materials are competitive only with the less effective filled and unfilled ceramic materials.

With one exception (Avcoat 5019) the low-temperature materials were polymer plastics without additives. Materials of this class have been evaluated extensively for heat of ablation (refs. 1, 2, and 3, for example). In reference 3 it was shown that nylon and an Avcoat material similar to Avcoat 5019 had comparatively high heat-of-ablation values, which increased with stream stagnation enthalpy. For low-temperature materials shielding is primarily due to latent heat of pyrolysis and injection of gaseous products of pyrolysis into the boundary layer, the latter being more effective at higher enthalpy. In the present investigation the great difference in performance between low-temperature ablators and charring ablators (many of which contain nylon) was primarily due to radiation from the char surface and absorption of heat as the gaseous products of ablation were raised from pyrolysis temperature to the char-surface temperature (ref. 5).

Epoxy-filled foamed zirconia (Martin Z-13)

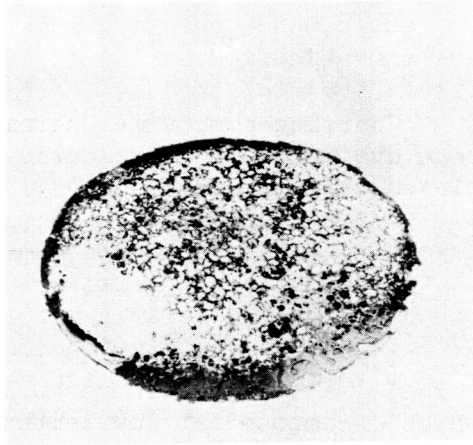

Before test

After test

Phenolic-filled foamed silicon carbide

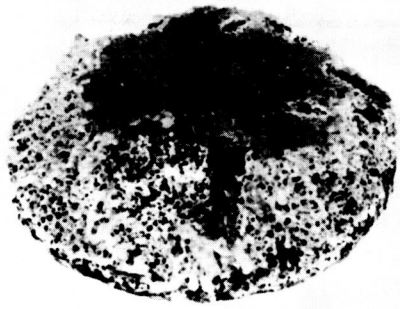

Before test

After test

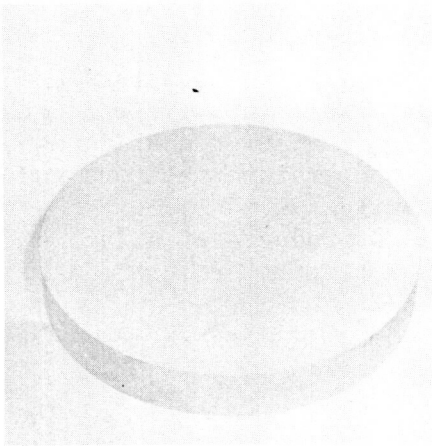

Phenolic-filled foamed silica (Avco RAD 58 B)

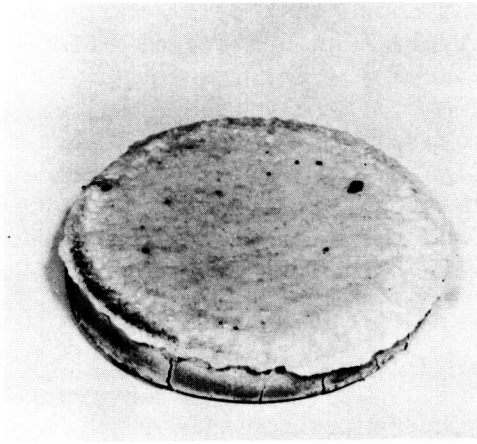

Before test

After test

Figure 9.- Typical ceramic materials. L-63-100

CONCLUDING REMARKS

Charring composite, ceramic, and low-temperature ablation materials have been evaluated in an electric-arc-heated subsonic airstream at constant stagnation enthalpy (approximately 3,000 Btu/lb), constant heating rate (approximately 100 Btu/ft^2-sec), and identical model configuration to compare effectiveness as thermal-protection systems for reentry applications involving long heating periods and high total-heat loads. The results of these tests have shown that:

1. Charring composite materials were significantly more effective than porous ceramic materials with an ablative filling or than thermal-protection materials which decomposed at low temperature. The comparison was based on a performance parameter which indicated the quantity of heat dissipated by a unit weight of material before the back-surface temperature reached a given value.

2. The most effective charring composite materials consisted of a phenolic resin combined with phenolic Microballoons to reduce density, nylon powder to increase gaseous boundary-layer shielding, and a small amount of silica to improve char integrity. Combinations with an epoxy resin and phenolic Microballoons were also effective.

Langley Research Center,
National Aeronautics and Space Administration,
Langley Station, Hampton, Va., April 5, 1963.

REFERENCES

1. Georgiev, Steven, Hidalgo, Henry, and Adams, Mac C.: On Ablating Heat Shields for Satellite Recovery. Res. Rep. 65 (AFBMD-TR-59-7), Avco-Everett Res. Lab., July 1959.

2. Steg, Leo: Materials for Re-Entry Heat Protection of Satellites. ARS Jour., vol. 30, no. 9, Sept. 1960, pp. 815-822.

3. Chapman, Andrew J.: An Experimental Investigation of Several Ablation Materials in an Electric-Arc-Heated Air Jet. NASA TN D-1520, 1963.

4. Warren, W. R., and Diaconis, N. S.: The Performance of Ablation Materials as Heat Protection for Re-Entering Satellites. Tech. Inf. Ser. No. R60SD316 (Contract AF 04(647)269), Missile and Space Vehicle Dept., Gen. Elec. Co., Feb. 19, 1960.

5. Brooks, William A., Jr., Swann, Robert T., and Wadlin, Kenneth L.: Thermal Protection for Spacecraft Entering at Escape Velocity. [Preprint] 513F, Soc. Automotive Eng., Apr. 1962.

6. Peters, Roger W., and Wilson, R. Gale: Experimental Investigation of the Effect of Convective and Radiative Heat Loads on the Performance of Subliming and Charring Ablators. NASA TN D-1355, 1962.

7. Gardon, Robert: An Instrument for the Direct Measurement of Intense Thermal Radiation. Rev. Sci. Instr., vol. 24, no. 5, May 1953, pp. 366-370.

8. Ahrens, L. H.: Spectrochemical Analysis. Addison-Wesley Pub. Co., Inc. (Cambridge, Mass.), 1954.

TABLE I.- OPERATING CHARACTERISTICS OF 2500-KILOWATT ARC-HEATED SUBSONIC AIR JET AT THE LANGLEY RESEARCH CENTER

Stream diameter, in.	4
Test medium	Air
Arc power (three-phase a-c), kw	1,560
Mass flow, lb/sec	0.35
Velocity, ft/sec	890
Mach number	0.21
Static enthalpy*, Btu/lb	3,000
Static pressure*, atm	1
Static temperature*, ^{o}R	7,200
Heat-transfer rate to 3-in-diameter flat surface, Btu/ft^2-sec	100 to 120
Maximum operating time	Continuous

*Approximate stagnation.

TABLE II.- SUMMARY OF TEST RESULTS FOR CHARRING COMPOSITE MATERIALS

Material	Composition		Density, ρ, lb/ft^3	Unit weight, m, lb/ft^2	Weight loss, m_a/m	Back-surface-temperature history							Heating rate (average cold wall), $\bar{q}$, Btu/ft^2-sec	Total heat load (cold wall), Q_o, Btu/ft^2	Effective heat capacity, Q_o/m, Btu/lb
						Exposure time		Termination of exposure			Maximum temperature rise				
	Component materials	Percent weight				t, sec for $\Delta T = 50^\circ$ F	t, sec for $\Delta T = 300^\circ$ F	t_f, sec	ΔT_f, $^\circ F$	$\left(\frac{dT}{dt}\right)_f$, $^\circ F/sec$	t_m, sec	ΔT_m, $^\circ F$			
PN-4*	Phenolic (BRP-5549) Nylon powder (Zytel) Phenolic Microballoons Eccospheres	15.8 63.4 15.8 5.0	36	3.03 3.00	96.7×10^{-2} 93.6	149 110	254 262	257 265	350 338	14.0 16.0	320 325	660 598	116.6 110.8	30,000 29,400	9,900 9,800
PN-3*	Phenolic (CTL-91LD) Nylon powder (Zytel) Phenolic Microballoons Eccospheres	23.0 47.0 25.0 5.0	36	2.99 3.06	94.3×10^{-2} 92.6	125 153	258 263	262 267	377 450	26.4 33.2	320 305	675 747	108.2 105.2	28,300 28,100	9,470 9,180
Chance Vought phenolic nylon	Phenolic Nylon Phenolic Microballoons Quartz		36	3.10	94.8×10^{-2}	170	291	296	375	14.9	339	605	98.8	29,200	9.420
Avcoat X5035	Epoxy Phenolic Microballoons Silica		37	3.00	79.2×10^{-2}	183	249	252	330	14.0	310	676	108.0	27,200	9,070
Narmco 3168	Epoxy Phenolic Silica		83	3.00 3.02	68.4×10^{-2} 54.0	88 104	215 238	220 235	315 290	3.8 8.7	300 327	475 424	114.0 106.3	25,100 25,000	8,370 8,280
PN-2*	Phenolic (BRP-5549) Nylon powder (Zytel) Phenolic Microballoons	25.0 50.0 25.0	36	3.00	95.1×10^{-2}	140	256	258	340	26.0	308	703	96.4	24,900	8,300
PB*	Phenolic (BRP-5549) Phenolic Microballoons	75 25	49	3.00 3.00	89.6×10^{-2} 100.0	151 178	227 210	230 213	333 376	15.6 29.8	290 270	700 730	103.0 110.0	23,700 23,400	7,900 7,800
Narmco 4505			80	3.00 2.99	80.0×10^{-2} 79.0	94 95	194 193	198 196	315 307	3.3 2.6	288 300	538 572	119.0 108.6	23,600 21,300	7,870 7,120
Chance Vought phenolic melamine	Phenolic Melamine Phenolic Microballoons Quartz		61	3.07	93.8×10^{-2}	147	238	239	318	14.5	275	515	100.0	23,900	7,790
Narmco 4018	Phenolic Nylon		74	2.98 2.98	92.4×10^{-2} 95.3	127 113	209 195	211 199	316 398	10.6 45.0	234 230	480 528	108.0 108.1	22,800 21,500	7,650 7,220
Chance Vought phenolic melamine	Phenolic Melamine Phenolic Microballoons Quartz		36	3.06	95.7×10^{-2}	130	238	239	316	16.0	287	575	96.5	23,100	7,550
Emerson Electric Thermo-Leg T-500 EX-167			86	3.00 3.62	67.8×10^{-2} 96.8	110 127	206 241	208 247	324 351	5.7 9.5	246 305	420 528	108.0 106.3	22,500 26,300	7,500 7,270
PAB*	Phenolic (BRP-5549) Ammonium chloride Phenolic Microballoons	25 50 25	45	3.00	100.0×10^{-2}	158	198	195	565	87.0	---	---	110.0	21,500	7,150
Avcoat X5032	Epoxy Phenolic Microballoons Silica		66	3.04	81.0×10^{-2}	126	195	198	346	14.8	250	620	107.0	21,200	6,970
PNG*	Phenolic (BRP-5549) Nylon powder (Zytel) Glass fiber	32.5 50.0 17.5	78	2.99	90.9×10^{-2}	114	185	188	346	16.4	221	538	110.5	20,800	6,950
Avcoat X5034	Epoxy Phenolic Microballoons Silica		65	3.10	92.3×10^{-2}	122	187	192	338	9.5	240	593	111.8	21,500	6,960

*Materials fabricated at the Langley Research Center. Designations used for convenience in identifying materials.

TABLE II.- SUMMARY OF TEST RESULTS FOR CHARRING COMPOSITE MATERIALS - Concluded

Material	Composition		Density, ρ, lb/ft^3	Unit weight, m, lb/ft^2	Weight loss, m_s/m	Back-surface-temperature history							Heating rate (average cold wall), $\bar{q}$, Btu/ft^2-sec	Total heat load (cold wall), Q_o, Btu/ft^2	Effective heat capacity, Q_o/m, Btu/lb
						Exposure time		Termination of exposure			Maximum temperature rise				
	Component materials	Percent weight				t, sec for $\Delta T = 50^o$ F	t, sec for $\Delta T = 300^o$ F	t_f, sec	ΔT_f, ^{o}F	$\left(\frac{dT}{dt}\right)_f$, ^{o}F/sec	t_m, sec	ΔT_m, ^{o}F			
Narmco 4503			80	3.00	92.9×10^{-2}	107	182	180	284	6.0	223	453	113.0	20,300	6,770
				3.02	92.6	106	178	182	372	17.3	240	615	107.9	19,700	6,520
PN-1*	Phenolic (BRP-5549) Nylon powder (Zytel)	50.0 50.0	75	2.96	88.5×10^{-2}	116	172	174	342	21.2	250	724	114.0	19,800	6,690
				2.99	87.9	111	167	172	478	39.4	250	752	116.6	20,100	6,720
GE Phenolic nylon glass	Phenolic Nylon Glass		82	3.04	83.6×10^{-2}	110	188	192	334	9.6	231	541	105.0	20,200	6,650
GE Phenolic nylon	Phenolic Nylon		75	3.02	92.5×10^{-2}	130	183	186	358	23.5	210	464	107	19,900	6,590
Narmco 4501			79	3.00	90.8×10^{-2}	82	170	176	346	6.4	215	461	111.0	19,500	6,500
GE 524-A	Epoxy Phenolic Microballoons		42	3.06	98.0×10^{-2}	168	184	186	458	171.0	---	---	106.0	19,700	6,440
GE 523-C	Epoxy Phenolic Microballoons		50	3.00	98.5×10^{-2}	155	176	178	444	89.0	---	---	108.5	19,300	6,430
GE 123-A	Epoxy		76	3.04	98.9×10^{-2}	136	174	176	410	61.9	---	---	109.5	19,300	6,350
GE 124-A	Epoxy		75	2.98	98.6×10^{-2}	142	175	178	1,120	36.2	---	---	106.0	18,900	6,340
PA*	Phenolic (BRP-5549) Ammonium chloride	50 50	85	3.00	91.5×10^{-2}	85	164	165	329	7.2	200	456	111.0	18,300	6,100
Avcoat X5026	Epoxy Phenolic Microballoons Silica		76	3.08	57.6×10^{-2}	97	153	162	390	12.1	230	732	111.4	18,000	5,840
				3.14	56.9	99	156	160	353	14.5	210	620	110.7	17,700	5,640
Narmco 4016			73	3.00	91.2×10^{-2}	115	151	155	359	25.9	185	583	111.0	17,200	5,730
Narmco 4504			85	3.00	96.4×10^{-2}	90	141	145	346	10.3	158	407	117.0	17,000	5,670
Narmco 4506			95	3.00	84.0×10^{-2}	80	147	148	310	6.8	186	438	111.0	16,400	5,470
Narmco 4502			93	3.00	85.6×10^{-2}	69	145	147	309	4.6	204	455	110.5	16,200	5,400
GE Phenolic refrasil	Phenolic Silica fiber		100	3.00	20.2×10^{-2}	57	142	149	334	5.3	240	630	107.0	15,900	5,300
GE 323-C	Epoxy Glass		96	3.02	83.5×10^{-2}	81	136	140	350	13.0	180	602	108.5	15,200	5,030
PAG*	Phenolic (BRP-5549) Ammonium chloride Glass fiber	32.5 50.0 17.5	96	2.98	90.8×10^{-2}	59	129	131	320	10.6	158	412	109.5	14,300	4,800
Narmco 4012	Phenolic Silica		105	3.00	16.3×10^{-2}	42	107	109	300	3.3	203	538	115.0	12,500	4,170
Phenolic* glass	Phenolic (BRP-5549) Glass fiber	70 30	90	3.04	59.7×10^{-2}	66	100	101	315	17.7	---	---	108	10,900	3,520
Narmco 4014			106	3.00	12.9×10^{-2}	39	89	91	308	5.3	184	615	109.0	9,920	3,310
Narmco 525-T4-VA			111	3.00	13.2×10^{-2}	30	72	74	316	8.2	150	663	114.5	8,470	2,820

*Materials fabricated at the Langley Research Center. Designations used for convenience in identifying material.

TABLE III.- SUMMARY OF TEST RESULTS FOR CERAMIC MATERIALS

Material	Composition	Density, ρ, lb/ft^3	Unit weight, m, lb/ft^2	Weight loss, m_a/m	Back-surface-temperature history							Heating rate (average cold wall), $\bar{q}$, Btu/ft^2-sec	Total heat load (cold wall), Q_o, Btu/ft^2	Effective heat capacity, Q_o/m, Btu/lb
					Exposure time		Termination of exposure			Maximum temperature rise				
	Component materials				t, sec for $\Delta T = 50^\circ$ F	t, sec for $\Delta T = 300^\circ$ F	t_f, sec	ΔT_f, $^\circ F$	$\left(\frac{dT}{dt}\right)_f$, $^\circ F/sec$	t_m, sec	ΔT_m, $^\circ F$			
Martin Z-13	ZrO_2 Epoxy	97	3.30	75.7×10^{-2}	95	165	167	314	6.4	240	540	115.9	19,400	5,880
Martin Z-14	ZrO_2 Epoxy	93	3.32	73.9×10^{-2}	98	173	176	320	5.2	235	540	100.6	17,700	5,120
Martin Z-1	ZrO_2 Phenyl-silane	72	3.14	39.1×10^{-2}	68	173	138	305	5.7	230	620	113.5	15,700	5,000
Martin Z-11	ZrO_2 Epoxy	97	3.20	76.0×10^{-2}	92	148	151	342	9.0	222	640	103.8	15,700	4,910
Martin A-6	SiC Phenyl-silane ZrO_2 coating on SiC	73	3.14	38.0×10^{-2}	49	140	145	326	5.4	245	642	103.0	14,900	4,750
Martin Z-12	ZrO_2 Epoxy	98	3.32	80.1×10^{-2}	88	144	149	353	8.2	223	605	104.3	15,500	4,670
Martin Z-8	ZrO_2 Phenolic	90	3.3	41.5×10^{-2}	76	126	132	340	5.2	202	550	115.0	15,200	4,610
Avco RAD 58 B	Si Phenolic	80	3.02	6.1×10^{-2}	58	122	127	325	4.8	220	580	108.7	13,800	4,570
Martin Z-7	ZrO_2 Phenolic	93	3.29	44.5×10^{-2}	91	142	144	312	6.3	219	570	104.0	15,000	4,560
Martin Z-10	ZrO_2 Phenolic	59	3.3	49.2×10^{-2}	88	141	141	300	5.5	227	545	106.5	15,000	4,550
Avco RAD 58 B (extended)	Si Phenolic Voids on back surface	57	2.98	2.7×10^{-2}	28	106	108	315	5.0	190	544	109.0	11,800	3,960
Martin Z-9	ZrO_2 Phenolic	60	3.31	47.3×10^{-2}	72	119	124	333	5.8	233	631	105.5	13,100	3,960
Martin A-5 (resin back)	SiC Phenolic ($\frac{1}{2}$ filled) ZrO_2 coating on SiC	60	3.02	23.0×10^{-2}	45	95	104	352	5.1	212	640	107.5	11,200	3,710
Martin Z-5	ZrO_2 Phenolic	91	3.29	34.8×10^{-2}	62	112	115	340	7.6	212	678	104.6	12,000	3,650
Martin A-15	Al_2O_3 Phenyl-silane	63	3.27	38.9×10^{-2}	37	102	102	300	6.7	200	728	116.0	11,800	3,610
Martin Z-15	ZrO_2 Phenolic	105	3.36	91.2×10^{-2}	68	100	102	341	10.8	149	535	105.5	10,800	3,210
Martin A-8 (resin back)	SiC Phenyl-silane ($\frac{1}{2}$ filled) ZrO_2 coating on SiC	57	2.96	21.4×10^{-2}	30	82	87	328	4.2	165	622	106.0	9,220	3,110
Martin A-13	Al_2O_3 Phenyl-silane	84	3.25	35.2×10^{-2}	33	92	89	292	5.6	185	647	111.0	9,880	3,040
Martin A-1	SiC	17	2.75	57.4×10^{-2}	38	80	81	305	8.2	135	520	103.0	8,340	3,030
Martin A-7	SiC Phenyl-silane ZrO_2 coating on SiC	54	3.27	36.2×10^{-2}	24	89	95	326	4.6	186	655	99.0	9,410	2,880
Martin A-5 (resin front)	SiC Phenolic ($\frac{1}{2}$ filled) ZrO_2 coating on SiC	61	3.04	24.8×10^{-2}	31	77	80	326	6.4	158	600	105.0	8,400	2,760
Martin A-12	Al_2O_3	36	2.75	73.2×10^{-2}	33	64	65	320	10.5	131	710	111.0	7,220	2,630
Martin A-8 (resin front)	SiC Phenyl-silane ($\frac{1}{2}$ filled) ZrO_2 coating on SiC	57	3.25	21.5×10^{-2}	25	71	77	349	6.5	152	667	106.0	8,160	2,510
Martin A-2	SiC ZrO_2 coating	59	3.04	22.2×10^{-2}	28	61	63	328	7.6	116	615	114.0	7,180	2,360
Martin A-4	SiC Phenolic ZrO_2 coating on SiC	50	3.16	33.2×10^{-2}	19	62	68	345	7.8	150	790	104.5	7,110	2,250
Martin A-10	SiC ZrO_2 coating	84	2.80	3.9×10^{-2}	30	49	50	308	7.4	139	546	115.5	5,780	2,060
Martin A-11	Al_2O_3	34	3.17	78.0×10^{-2}	23	52	54	322	8.5	126	575	115.0	6,210	1,960
Avcoat I	Si Metallic additives Inconel honeycomb reenforced	146	3.02	0.7×10^{-2}	13	32	36	360	14.8	40	---	104.0	3,740	1,240

TABLE IV.- SUMMARY OF TEST RESULTS FOR LOW-TEMPERATURE MATERIALS

Material	Density, ρ, lb/ft^3	Unit weight, m, lb/ft^2	Weight loss, m_n/m	Back-surface-temperature history							Heating rate (average cold wall), $\dot{q}$, Btu/ft^2-sec	Total heat load (cold wall), Q_o, Btu/ft^2	Effective heat capacity Q_o/m, Btu/lb
				Exposure time		Termination of exposure			Maximum temperature rise				
				t, sec for $\Delta T = 50^\circ$ F	t, sec for $\Delta T = 300^\circ$ F	t_f, sec	ΔT_f, $^\circ F$	$\left(\frac{dT}{dt}\right)_f$, $^\circ F/sec$	t_m, sec	Δt_m, $^\circ F$			
Polyethylene	61	3.03	100.0×10^{-2}	66	72	74.0	1,120	371			111.0	8,200	2,700
Nylon	72	2.96	100.0×10^{-2}	50	57	60.0	1,000	248			108.5	6,500	2,200
Avcoat 5019	68	3.06	99.3×10^{-2}	53	54	58.0	1,880	397			110.0	6,380	2,090
Teflon	135	3.00	100.0×10^{-2}	23	45	49.0	-----	---			112.5	5,500	1,830
Teflon (low density)	87	3.00	100.0×10^{-2}	44	46	49.0	1,345	476			110.5	5,400	1,800